Proceedings of ASME Turbo Expo 2011
GT2011
June 6-10, 2011, Vancouver, British Columbia, Canada

GT2011-45244

EXPERIMENTAL AND NUMERICAL INVESTIGATION OF THE UNSTEADY FLOW FIELD AND TONE GENERATION IN AN ISOLATED CENTRIFUGAL FAN IMPELLER

Daniel Wolfram
POLLRICH Ventilatoren GmbH
41065 Mönchengladbach
Germany

Thomas H. Carolus
University of Siegen
Department of Fluid- and Thermodynamics
57068 Siegen, Germany

ABSTRACT

In spite of low circumferential Mach number the sound of isolated centrifugal fan impellers is sometimes dominated by distinctive tones at blade passing frequency (BPF) and integer multiples. This paper reports on an experimental and numerical investigation intended to unveil the tone generating mechanism. The sound spectra from three impellers operating at a large range of speed were measured and decomposed into Strouhal and Helmholtz number dependent functions. This led to the preliminary conclusion that the BPF related tones are exclusively flow-induced. Based on hot-wire and blade pressure fluctuation measurements and a subsequent correlation analysis, coherent flow structures different from the one associated with the principal azimuthal flow pattern due to the blades were detected. Eventually, numerical three-dimensional unsteady flow simulation and experimental flow visualization revealed an inlet vortex. It takes on a helical form, with the vortex core slowly varying its position with respect to the impeller center. As the blades cut through that quasi-stationary helical vortex they encounter blade force fluctuations producing the BPF tones. The slow spin of the vortex core and the slow variation of vortex strength were identified as the reason for the amplitude modulation of the BPF tone.

NOMENCLATURE

a	speed of sound
c	flow velocity in the stationary frame of reference
b_1	impeller width at intake
b_2	impeller width at discharge
C, C_{xy}	coherence function
d_1	impeller intake diameter at blade leading edge
d_2	impeller diameter (at blade trailing edge)
F	function of Sr within spectral decomposition
G	function of He within spectral decomposition
He	Helmholtz number
l	chord length
L	level (in dB)
f	frequency
Ma	circumferential Mach number based on u_2
m	azimuthal mode order
n	speed
p	static pressure, sound pressure
Re_d	Reynolds number based on d_2 and u_2
Sr	Strouhal number
t	time
u	circumferential velocity of impeller
$\dot{V}$	volume flow rate
w	flow velocity in the rotating frame of reference
W	sound power
z	number of blades
ζ_{xy}	phase angle between two signals x and y
η_{ts}	total to static efficiency
θ_{xy}	angular spacing angle of two probes x and y
λ	shaft power coefficient
ν	kinematic viscosity
ξ_{11}, ξ_{12}, ξ_3	blade coordinate system (rotating frame of reference)
φ_r	flow rate coefficient
ψ_{ts}	total to static pressure rise coefficient

Subscripts and Superscripts

0	reference value
1	at intake (leading edge)
2	at discharge (trailing edge)
Int	interaction
Mod	mode
opt	at design point
p	pressure
S	shaft
sp	surface pressure
W	sound power
*	non-dimensionalized

Abbreviations

BPF	blade passing frequency
CFD	computational fluid dynamics
LM100	100% size impeller
LM75	75% size impeller
LM50	50% size impeller
LE	leading edge
TE	trailing edge

1. INTRODUCTION

Centrifugal fans are used for their ability to generate a relatively high total pressure rise at a reasonable compact size. Aiming at a high static pressure rise one can spare a volute or a vaned outlet diffusor if the impeller is designed for a high degree of reaction by selecting small blade angles and other appropriate dimensions. Typical applications of centrifugal fans consisting merely of an impeller and a stationary inlet nozzle are in Heating-Ventilating-Air Conditioning (HVAC-) systems, cooling units in trains, ventilating systems for clean rooms, etc. The noise generated in centrifugal fan impellers in general is both broadband and tonal. Broad band components are due to separated flow at the impeller shroud (i.e. at front plate of the closed impeller as the flow turns from the axial into the radial direction), turbulent and/or secondary flow in the blade channels and flow/blade trailing edge interaction (Fehse et al. [1], Choi et al. [2]).

Studies on rotating stall in centrifugal impellers resulting in tonal type noise are numerous. An early investigation was done by Gottschalk [3]. When the impeller is operated in the part load range the flow in one or more blade channels stalls and blocks off the flow in those channels. The through flow velocity in the remaining channels increases and ensures stall free flow. Those stall cells, however, are non-stationary with respect to their circumferential position in the impeller. They travel in the stationary frame of reference in the same direction as the impeller but with reduced speed. Mongeau et al. [4, 5] investigated the sound generated by rotating stall in an impeller. They found that the aerodynamic interaction between a rotating stall pattern and the blades dominates the low frequency noise production and is responsible for peaks in the acoustic signature. Among others they constructed the rotating flow field pattern from the signals of two stationary hot wire probes. Tetu et al. [6] identified two types of tones produced by the interaction of blades with modes of the coherent large scale instability: i) a tone produced at the same frequency as an identified component of the large scale velocity field instability, ii) tones at other frequencies generated by an interaction between the flow field fluctuating components at the instability frequencies and the shaft rate frequency. Other work was done by Fringe and Van den Braembussche [7], Pavesi et al. [8]. The typical frequency of rotating stall noise ranges from 60 to 80% of BPF but never equals BPF or its harmonics [9].

Isolated centrifugal impellers should not exhibit tonal noise at blade passage frequency (BPF) typically associated with the interaction between the periodic blade channel flow and guide vanes or the volute cuttoff. However, as manufacturers and customers report and as measurements confirm (Fig. 1), some designs may suffer from tonal noise at BPF. Simplistically these tones may be attributed to the blade forces due to the flow deflection in the blade channel. Those forces are associated with the change of angular momentum, the working principle of any turbomachine. They are stationary with respect to each rotating blade and thus form a rotating pressure field as they rotate. However, as shown by many authors, the sound radiated by those rotating forces is marginal as long as the circumferential Mach number (i.e. the circumferential speed at the impeller outlet over the speed of sound) of the impeller is far subsonic (Lowson [12], Wright [13], Roger [14], Goldstein [15], Blake [16]). This is the case for most low pressure fans. To the knowledge of the authors, no work has been done on the noise at BPF from isolated centrifugal fan impellers. Thus the objective of this study is to characterize the noise in a controlled laboratory environment and eventually to shed some light on the noise generating mechanism.

In some cases a secondary flow between the stationary inlet nozzle and the impeller inlet creates a very dominant high frequency whistling sound, Fig. 1. This is not covered in this paper, since it can be avoided by giving the nozzle-gap region a small asymmetric geometry, see e. g. Deutsches Gebrauchsmuster [11].

2. FANS INVESTIGATED AND TEST RIG

Three geometrically similar impellers, as depicted in Fig. 2 and specified in Tab. 1, have been manufactured and investigated. Each of them has z = 6 blades. The blades are swept backwards with a two-dimensional curvature. In order to avoid the typical mass production tolerances the manufacturing process was controlled carefully. So the three impellers are nearly perfectly similar with respect to their geometry. Spark machining enabled even the blade thickness to be scaled accurately.

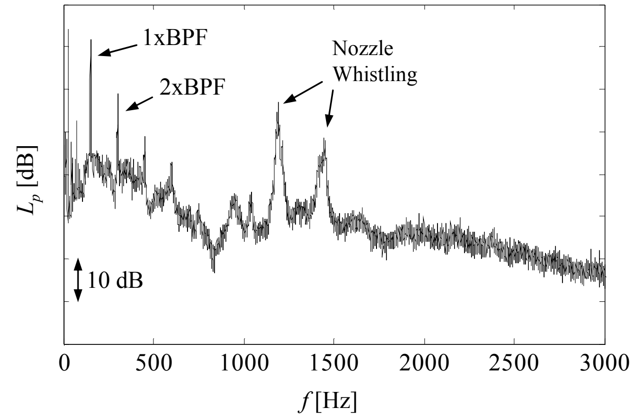

Fig. 1. Noise spectra of an isolated centrifugal impeller near design point; d_1/d_2 = 0.682, b_2/d_2 = 0.285, z = 6, n = 1500 1/min, dominant tones are at multiples of BPF and at high frequency due to nozzle whistling; tones and the whistling are not related to each other, Wolfram [10]

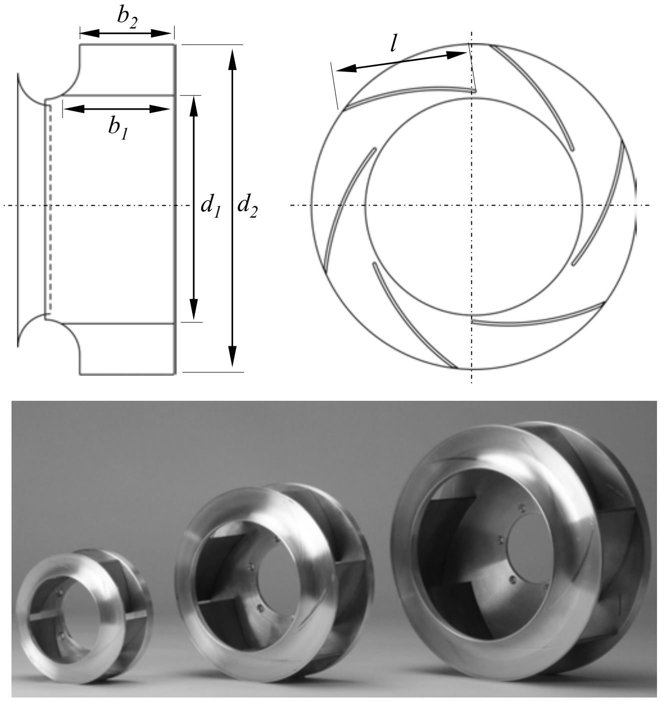

LM050 (50%) *LM075* (75%) *LM100* (100%)

Fig. 2. Impeller/stationary bellmouth nozzle and the three geometrically similar impellers manufactured

Tab. 1. Important impeller parameters

		LM100	LM075	LM050
Intake diameter	d_1 [mm]	242	182	121
Impeller diameter	d_2 [mm]	355	266	178
Impeller width at d_1	b_1 [mm]	113	84	57
Impeller width at d_2	b_2 [mm]	101	76	51
Blade chord length	l [mm]	150		

The impeller takes the air from a large semi-anechoic room via an inlet nozzle and exhausts into a pressure plenum with acoustically damped walls, Fig. 3. A duct with an anechoic termination is mounted on the chamber's pressure side. The operating point is controlled by a throttle downstream of the termination. The flow rate is measured by a hot film probe in the duct. The sound pressure is measured in the anechoic room by a calibrated microphone (Brüel & Kjær type 4190) at r_s = 1 m in front of the inlet nozzle on the axis of rotation. Preliminary experiments showed no pronounced angular dependency of sound pressure at BPF. The sound power is calculated assuming the sound pressure being equal on a hemispherical surface surrounding the inlet. Although this simplification will not yield accurate sound power levels, it is thought to be sufficient for comparing acoustic effects within this study. The reference pressure is $p_0 = 2 \cdot 10^{-5}$ Pa and the reference sound power $W_0 = 10^{-12}$ W. The same value is taken as reference for the levels of the surface pressure measurements in sections 4 and 5. All overall levels are the sum of narrow band levels from 50 Hz to 10 kHz. For the spectral analysis of all data MATLAB® routines (Version 7.0.4, R14) of the The Mathworks Inc. are employed. E.g., the power spectral density of an signal $x(t)$ is obtained with the routine pwelch with the parameter setting window = hann(nfft), noverlap = round(nfft/2) with nfft = round(T/8). If not otherwise stated, the length of all measured time signals is T = 30 s. Thus, we obtain a frequency resolution of $\Delta f = 8/T = 0.266$ Hz in all spectra.

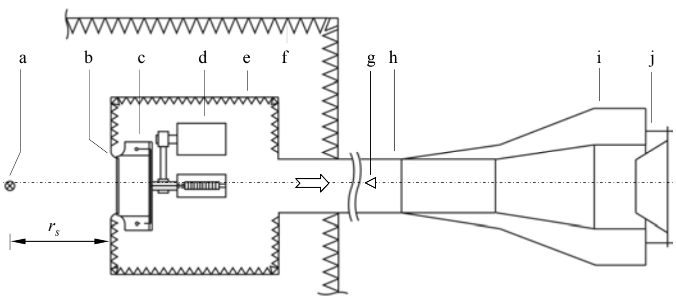

Fig. 3. Test rig; *a* microphone, *b* inlet nozzle, *c* tested impeller, *d* drive with belt transmission, *e* pressure plenum, *f* anechoic room, *g* hot film probe, *h* duct with *i* anechoic termination, *j* adjustable throttle

3. FAN PERFORMANCE

3.1 Aerodynamic Performance

Unlike from all the other experiments the aerodynamic curves of operation were determined employing a standard plenum test rig for fans according to the German standard DIN 24163 [17]. The following non-dimensional fan performance parameters are used:

- flow rate coefficient

$$\varphi_r = \frac{\dot{V}}{\pi^2 d_2^{\,2} b_2 n} \tag{1}$$

- total to static pressure rise coefficient

$$\psi_{ts} = \frac{2\Delta p_{ts}}{\pi^2 d_2^{\,2} \rho n^2} \tag{2}$$

- shaft power coefficient

$$\lambda = \frac{8 P_S}{\pi^4 d_2^{\,5} \rho n^3} \tag{3}$$

- total to static efficieny

$$\eta_{ts} = \frac{\dot{V}\Delta p_{ts}}{P_S} \tag{4}$$

For the three impellers the speed was set individually to obtain the same value $4.37 \cdot 10^5$ of the Reynolds number

$$\mathrm{Re}_d = \frac{u_2 d_2}{\nu} = \frac{\pi n d_2^{\,2}}{\nu} \tag{5}$$

The non-dimensional aerodynamic performance curves collapse nearly perfectly. Only the 50% impeller shows some small deviation at part load. For future reference the design point is defined as the point of operation with maximum total to static efficiency, i.e. at $\varphi_{r,\mathrm{opt}}$ = 0.15.

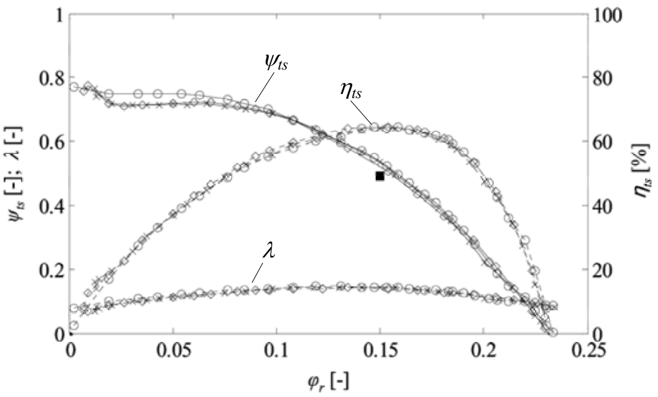

Fig. 4. Non-dimensional aerodynamic performance curves of the three impellers LM100, LM075 and LM050; ■ denotes a result from the numerical analysis in section 5

3.2 Acoustic performance

Fig. 5 shows the sound pressure time signal and part of the sound power spectrum in the vicinity of BPF as radiated from the 100% impeller at n = 1000 rpm. The time signal reveals clearly the periodic fluctuations associated with BPF. The amplitude of the tone, however, varies more or less randomly with time. Taking instantaneous short interval spectra of the time signals it becomes obvious that the sound pressure level varies by up to 15 dB within 30 seconds. This large scale amplitude modulation of the BPF tone is distinctly audible. The time averaged spectrum within a larger frequency range is similar to the one shown in Fig. 1. In spite of this unsteadiness of sound production we will discuss time averaged spectra in the remainder of the paper if not otherwise indicated.

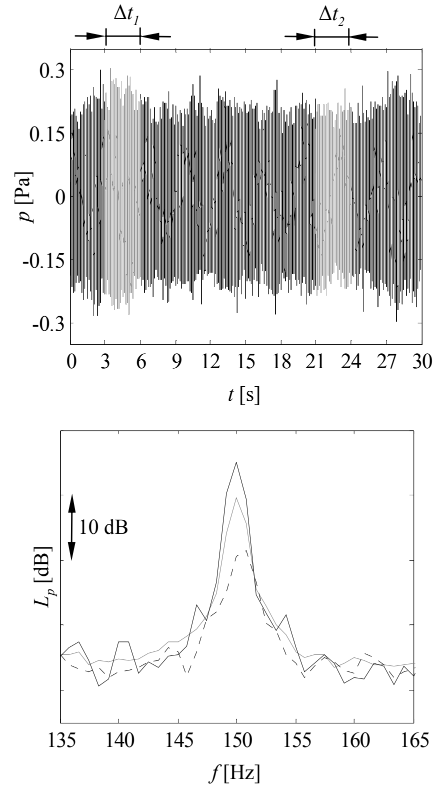

Fig. 5. Sound pressure at distance r_s from the impeller LM100 operating at design point; upper: time signal of measured sound pressure; lower: time averaged sound pressure spectra of the entire interval (—) and instantaneous short interval spectra for Δt_1 (—) and Δt_2 (---)

In order to reveal fundamental characteristics of the radiated sound the sound power of these three impellers was determined for a range of rotational speeds from 500 up to 4000 rpm while varying the aerodynamic point of operation from partial load via the design point to overload. The spectra have been further analyzed employing Weidemann's spectral decomposition technique (Weidemann [18], Mongeau [5]). For that non-dimensional parameters have been derived from a standard dimensional analysis. Seven parameters are considered essential to describe the BPF tone problem: Sound power W with its unit [W], speed of sound a [m/s], acoustic frequency f [Hz], volume flow rate $\dot{V}$ [m³/s], rotational speed n [rpm], impeller diameter d_2 [m] and the density of the fluid (here the air) ρ [kg/m³]. The acoustic frequency can be written in terms of the acoustic wave length λ as $f = a/\lambda$. In addition the (dimensionless) number of impeller blades z is added to the list. Possible effects of the air viscosity and thus friction effects are neglected. Eventually one obtains four independent non-dimensional parameters as summarized in Tab. 2. The Strouhal number is defined such that Sr = 1 corresponds to BPF, 2 to 2x BPF etc. Note that the Helmholtz number is not an independent parameter but arises from a combination of Strouhal and Mach number. The Helmholtz number is valuable for the forthcoming discussion. The non-dimensional sound power spectra are decomposed in form of the product of two non-dimensional functions F and G, each being only a function of the Strouhal or the Helmholtz number, respectively:

$$W^* = F^2(\mathrm{Sr}) \cdot G^2(\mathrm{He}) \tag{10a}$$

or in terms of a level

$$L_{W^*} = 10\log F^2(\mathrm{Sr}) + 10\log G^2(\mathrm{He}) \quad \mathrm{dB} \tag{10b}$$

A Strouhal number dependency would be characteristic for flow induced sound sources, whereas a Helmholtz dependency indicates effects of resonance and propagation.

Tab 2. Non-dimensional parameters

Normalized sound power	$W^* = \dfrac{W}{d_2^{\,5} n^3 \rho}$ $L_{W^*} = 10\log W^*$ dB	(6)
Circumferential Mach number	$\mathrm{Ma} = \dfrac{u_2}{a} = \dfrac{\pi d_2 n}{a}$	(7)
Flow coefficient for centrifugal fans	$\varphi_r = \dfrac{\dot{V}}{\pi^2 d_2^{\,2} b_2 n}$	(1)
Strouhal number	$\mathrm{Sr} = \dfrac{f}{nz} = \dfrac{f}{BPF}$	(8)
Helmholtz number	$\mathrm{He} = \mathrm{Sr} \cdot \mathrm{Ma} \cdot \dfrac{z}{\pi} = \dfrac{d_2}{\lambda} = \dfrac{d_2 f}{a}$	(9)

Fig. 6 contains all measured and non-dimensionalized spectra $L_{W^*}(f)$ from all three impellers at their design point $\varphi_{r,\mathrm{opt}} = 0.15$ at various rotational speeds. The decomposition clearly reveals that (i) A decomposition according to Eqs. (10) works and (ii) Tones at BPF and their higher harmonics are a function of Strouhal but not of Helmholtz number. This leads to the conclusion that the BPF related tones are exclusively flow-induced. There is no evidence of a resonance phenomenon as a Helmholtz number dependency would indicate. Surprisingly, unlike phenomena such as rotating stall or nozzle whistling, the level of the BPF tones are nearly independent of the fan aerodynamic point of operation, Fig. 7.

4. MODAL ANALYSIS

The previous results led to the hypothesis that a so far unidentified secondary flow structure exists which interacts with the rotating impeller blades and causes fluctuating blade forces acting as an acoustic dipole source. This hypothesis is checked by a modal analysis of the near-blade flow field. A similar procedure, though applied to a different sound phenomenon, had been described by Bent [19] and Tetu et al. [20], see also Bendat and Piersol [21].

4.1 Theoretical Background

Coherent secondary flow structures at the inflow and/or the discharge of a centrifugal impeller can be thought as wave patterns along the circumference, so-called azimuthal modes. These modes may interact with the principal flow pattern associated with the blade channels rotating at rotor speed n. If the rotational speed of the modal wave pattern n_{Mod} differs from n, interactions occur every time a wave peak hits a blade edge. A special case is a steady mode, i.e. non-rotating in the stationary frame of reference.

An azimuthal mode and its interaction are characterized by three parameters: The rotational speed of the wave pattern n_{Mod}, the mode

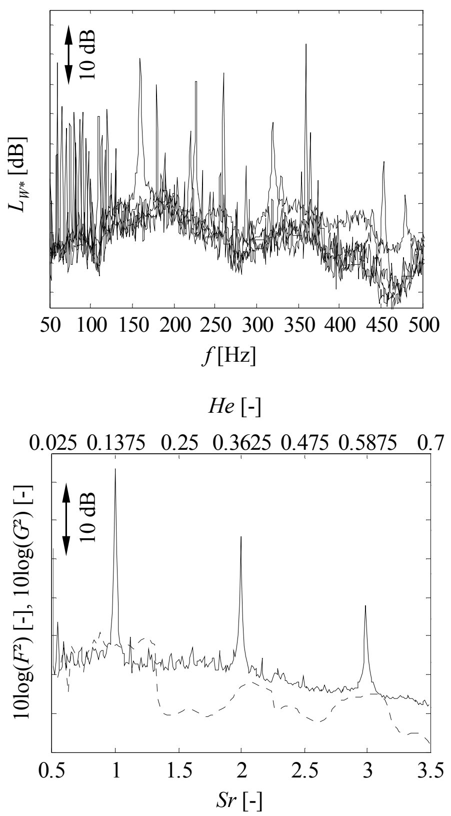

Fig. 6. Spectral decomposition of the measured sound power spectra from the three to scale centrifugal impellers at design point $\varphi_{r,opt}$ = 0.15 at various rotational speeds; (a) non-dimensional power spectra; (b) squared functions *F*(Sr) (—) and *G*(He) (---)

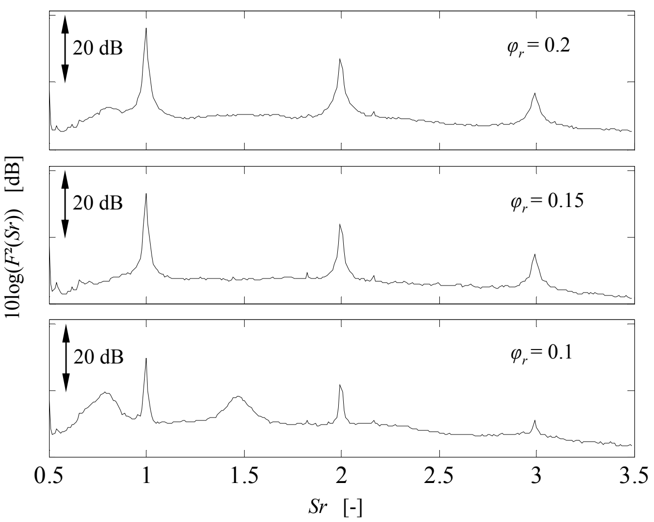

Fig. 7. *F*(Sr)-function of the impeller LM100 operating at (a) overload, (b) design point, (c) part load

order m, i.e. the number of waves along the impeller's circumference, and the frequency of blade-mode interaction f_{Int}, which eventually may correspond to the frequency of an acoustic tone radiated. Fig. 8 illustrates an arbitrary example. Since the impeller has six blade channels the principal flow pattern - rotating with the impeller's rotational speed n - is of 6th order, i.e. it has six lobes. The anticipated secondary flow structure has the shape of an azimuthal mode of order m = 5, hence five lobes. It rotates with the so far unknown rotational speed n_{Mod}.

Detecting and characterizing azimuthal modes requires at least two signals $x(t)$ and $y(t)$ of a flow field variable, measured synchronously at different circumferential positions spaced at a known angular distance θ_{xy} apart. The analysis used here is in the frequency domain. First, the power spectral densities $S_{xx}(f)$, $S_{yy}(f)$ and the cross power spectral density $S_{xy}(f)$ are determined from the time signals. Since azimuthal modes are assumed to be coherent flow structures a large value of the coherence function

$$C_{xy}(f) = \frac{\left|S_{xy}(f)\right|^2}{S_{xx}(f) \cdot S_{yy}(f)} \tag{11}$$

serves as an indicator. (The coherence function varies from 0 to 1). Then the ratio of imaginary to real part of the cross power spectral density yields the phase angle between both signals:

$$\zeta_{xy} = arctan\left(\frac{Im\left\{S_{xy}\right\}}{Re\left\{S_{xy}\right\}}\right) \tag{12}$$

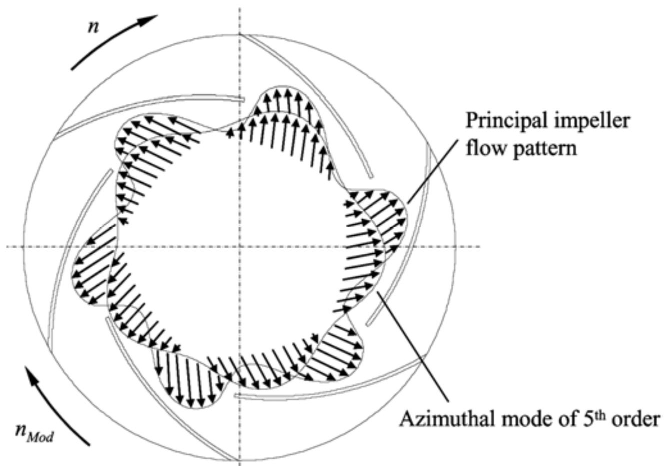

Fig. 8. Example: A 5th order mode interfering with the 6th order principal flow pattern at the inflow of a centrifugal impeller (schematically)

Since the phase angle is bounded at +/-180 degrees the effective phase angle may differ from the measured one by an integer multiple of 360 degrees. Eventually the mode order is derived from the phase angle and the circumferential angle between the two data acquisition points as

$$m = \frac{\zeta_{xy}}{\theta_{xy}} \tag{13}$$

The rotational speed of the azimuthal mode, measured by stationary probes, then becomes

$$n_{\mathrm{Mod}} = \frac{f}{m} = n\left(\frac{Sr \cdot z}{m}\right) \tag{14}$$

whereas measured by probes rotating with the impeller

$$n_{\mathrm{Mod}} = n - \frac{f}{m} = n\left(1 - \frac{Sr \cdot z}{m}\right) \tag{15}$$

Eqs. (14) and (15) require n_{Mod} to be a positive fraction of n. As a mode travels along one impeller circumference each of the m lobes interacts one time with each blade, i.e. the total number of interactions is

$$N_{\mathrm{Int,total}} = mz \tag{16}$$

However, some lobes and blades may interact simultaneously and hence do not contribute to the acoustically relevant frequency of interaction. The number of mode-blade interactions N_{Int}, which does not contain multiple interactions, can be found via a simple select and count routine. Eventually, both the number of those interactions and the mode's rotational speed yield the acoustically relevant frequency of mode-blade interaction

$$f_{\mathrm{Int}} = N_{\mathrm{Int}}\left(n - n_{\mathrm{Mod}}\right) \tag{17}$$

Corresponding to the definition of the Strouhal number a non-dimensional frequency of interaction is defined as

$$f_{\mathrm{Int}}{}^{*} = \frac{f_{\mathrm{Int}}}{\mathrm{BPF}} \tag{18}$$

Ambiguity of the result may be reduced by analyzing the unsteady flow field with more than just one pair of sensors.

Note that modes can only be discovered when they move relative to the probes. Hence probes in the stationary laboratory system are unable to detect modes which are stationary laboratory system. By contrast, probes fixed to the rotating impeller system can not detect modes which rotate at the same speed as the impeller.

4.2 Instrumentation

Each impeller blade of the 100% impeller has been instrumented with seven flush mounted miniature pressure transducers (Knowles Acoustics type FG-3329-P07), Fig. 9. ξ_3 is the chordwise coordinate normalized with the chord length, ξ_{11} and ξ_{11} are the spanwise coordinates normalized with the rotor width at intake and discharge, respectively. The pressure transducers have been calibrated in situ. A slip ring transducer transfers the signals from the rotating impeller system to the non-rotating laboratory system. Both, the random noise from the slip ring transducer and the acceleration of the transducers due to the rotary motion are found to be negligible. Signals from three pairs of transducers at an angular spacing $\theta_{xy} = 60°$, $\theta_{yz} = 180°$ und $\theta_{xz} = 240°$, inevitably given by the blade spacing, have been acquired simultaneously.

The unsteady inflow velocity to the impeller blade is measured by three stationary one-dimensional hot wire probes (Dantec Dynamics type 55P15/55H20), Fig. 10. The probes are mounted from the back of the intake through the hollow rotating shaft and the hub in order to not disturb the inflow. Their angular spacing is set to 30°, 45°, and 75°, respectively. The three probes can be traversed en bloc in axial direction from hub to shroud. Although the direction of the flow at the probes' location is not known a priori the wires are oriented normal to the circumferential direction. The expected inaccuracy in the absolute velocity readings due to the potential misalignment is not decisive, since it will have minor effect on the space-time correlation the measurements are aimed at. A similar arrangement of hot wire probes is applied to the impeller discharge (Wolfram [22]). The hot wire signals are captured synchronously by a standard multi-channel constant-temperature anemometer system (Dantec CTA StreamLine) in connection with an appropriate data acquisition system. In addition, the acoustic signal from the microphone as in Fig. 3 has been recorded synchronously. Further details of the various test rigs are described in [22] and [23]. For the interpretation of the results it is important to know that the impeller speed was always set to 1500 rpm = 25 Hz. The fan was always operating at its design point $\varphi_{r,\mathrm{opt}} = 0.15$.

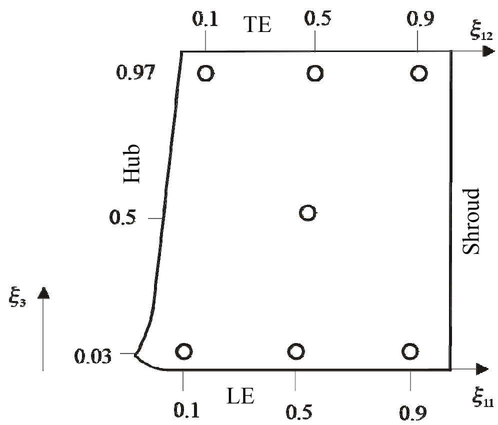

Fig. 9. Locations of the flush mounted miniature pressure transducers on the blade surface; LE = leading, TE = trailing edge

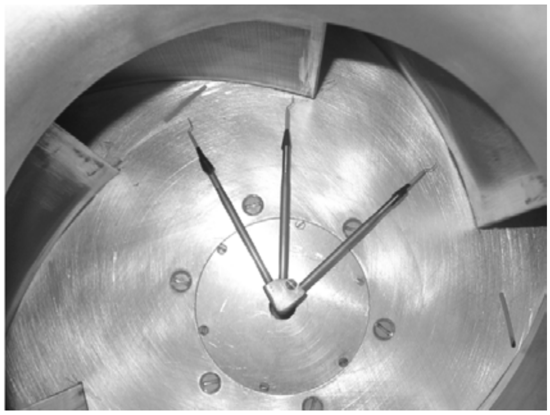

Fig. 10. Three stationary hot wire probes in the impeller inlet; common shaft through hollow shaft and back plate

4.3 Results

By evaluating measured time records from pairs of stationary hot-wire and rotating blade surface pressure transducers one obtains coherence and phase data as shown in Fig. 11. The coherence function indicates consistently high coherence at discrete values of Sr. The values depend on whether the data originates from a stationary or rotating set of probes. High coherence is taken as an indicator for the existence of an azimuthal mode.

Further evaluation reveals the mode orders and their rotational speed as shown in Fig. 12. Clearly there exist modes of order 1 to at least 12. They either travel (i.e. rotate) with the same speed as the impeller or they are nearly stationary with respect to the laboratory system. The rotating modes are obtained from the stationary hot-wire probes. As pointed out earlier, modes traveling with the impeller speed $n_{\mathrm{Mod}} = n$ = 1500 rpm can not interact with the principal flow and hence are not candidates for acoustic sources. Here they represent merely the principal flow pattern in the impeller. On the other hand, the stationary modes (n_{Mod} = 0 rpm), as detected by the rotating pressure probes, may well interact with the blade.

The middle graph in Fig. 13 indicates the number of mode-blade interactions detected while evaluating the 30 s time records. Most frequently an interaction is encountered at f_{Int}^* = Sr = 1. This nicely coincides with the tone produced at Sr = 1 (i.e. at BPF) in the acoustic spectrum, upper graph in Fig. 13. Less frequently but still pronounced interactions exist at higher harmonics. Fig. 13 (bottom) proves that the coherence of the underlying pairs of signals is nearly perfect at those values of Sr. The associated azimuthal modes are the ones which do not rotate (n_{Mod} = 0 rpm, see Fig. 12). By contrast the modes detected as rotating with 1500 rpm yield frequencies of interaction f_{Int}^* = Sr = 0.9, 3.8 and 4.8. The coherence of the underlying signals is remarkably lower and, as one might expect, their contribution in the sound power spectrum is negligible or non-existent.

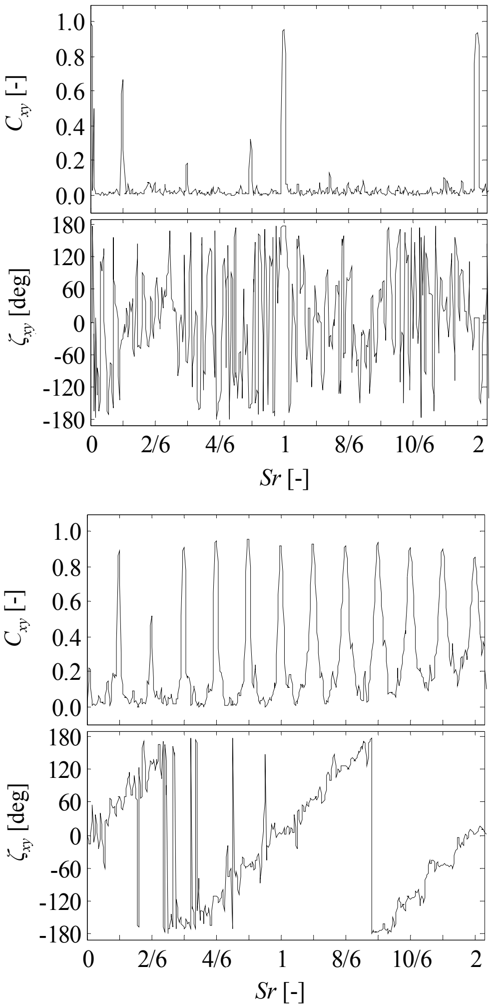

Fig. 11. Example: Coherence and phase data at intake; upper: from a pair of stationary hot-wire probes, lower: from a pair of blade surface pressure transducers

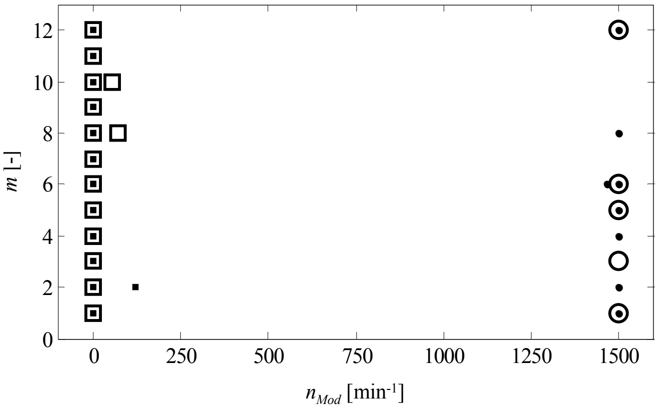

Fig. 12. Detected azimuthal modes: Order *m* and mode rotational speed n_{Mod}; originating from velocity at intake ○, at discharge •; pressure at intake □, at discharge ▪

The results so far are based on measurements from the impeller intake region. Although not shown here similar results have been obtained at the discharge region. In principle the modal analysis is not able to identify any causality. The azimuthal modes may be caused by flow structures either at the intake or the discharge or even within the blade channels. Fig. 14 shows the pressure levels at various locations on the blade surface (cp. Fig. 9). Evidently the pressure peaks at the leading edge are 5 to 20 dB higher as compared to the trailing edge (i. e. at the discharge region). Likewise the highest surface pressure levels are found close to hub where the axial inflow impinges. This leads to the suspicion that the coherent flow structures are predominant in the intake. The correlation of pressure sensor signals in the chordwise direction from the leading to the trailing edge supports this hypothesis, Fig. 15: Coherent structures of a large range of Sr number (i.e. length scales) are convected with a constant velocity

$$c_c = \frac{-2\pi f l_{xy}}{\zeta_{xy}} \tag{19}$$

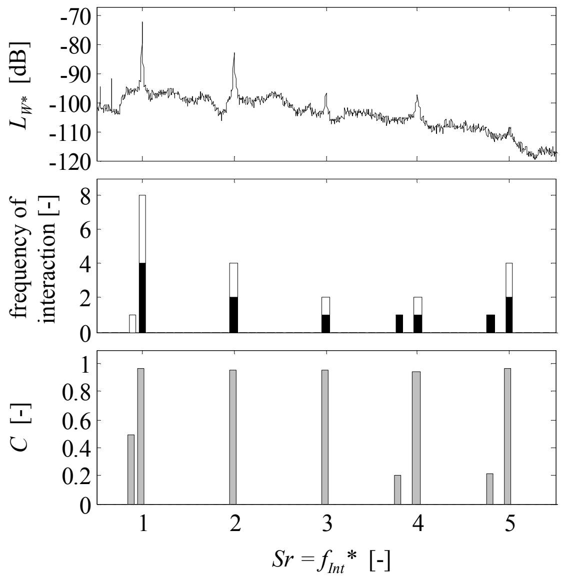

Fig. 13. Azimuthal modes; upper: measured normalized sound power spectrum; middle: frequency of mode-blade-interaction at inflow (black bars) and discharge (white bars); lower: Coherence

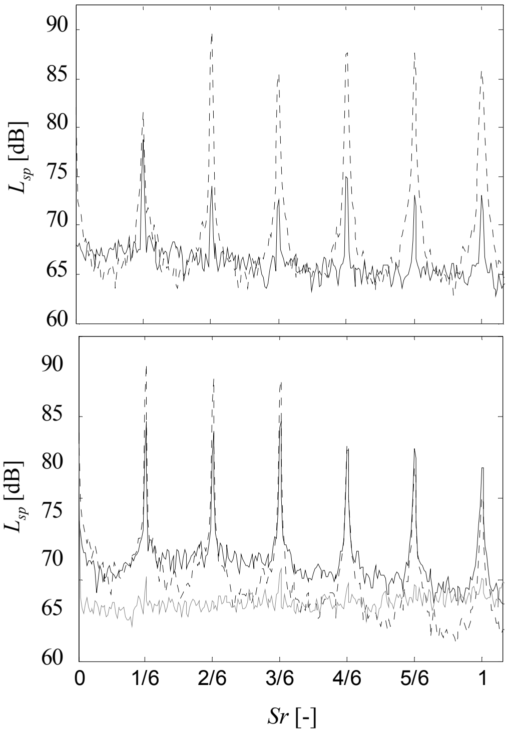

Fig. 14. Measured distribution of blade pressure fluctuations. Upper: in chordwise direction at ξ_3 = 0.03 (i.e. at the leading edge) (---) and ξ_3 = 0.97 (i.e. at the trailing edge) (—) at ξ_{11} = ξ_{12} = 0.5; lower: in axial direction along the leading edge at ξ_{11} = 0.1 (—), ξ_{11} = 0.5 (—), ξ_{11} = 0.9 (---)

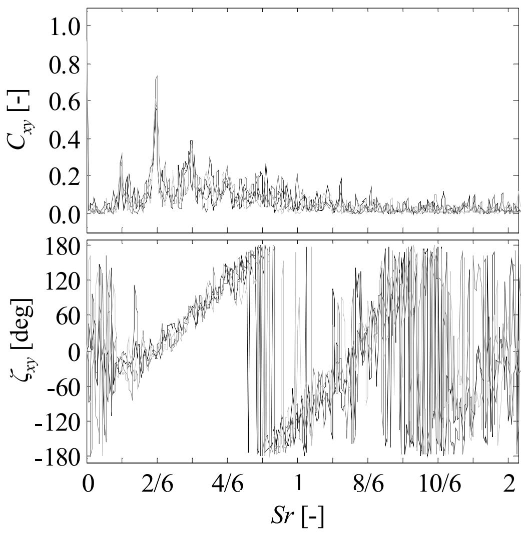

Fig. 15. Convection of coherent flow structures: Coherence and phase data from measured blade pressure fluctuations between intake and discharge

where l_{xy} is the spacing between the two sensors. Numerical evaluation of the convection speed gives values which coincide well with the through flow velocity as simply obtained from blade channel cross sectional area and volume flow rate.

The overall conclusions from the modal analysis and the extended signal correlation are: (i) Coherent flow structures exist; (ii) Presumably they originate in the intake and are convected through the blade channels to the discharge of the impeller; (iii) They are steady or at least quasi-stationary with respect to the laboratory system; (iv) They interact with the rotating blades and cause periodic blade force fluctuations which exactly match the frequency of the radiated tones, namely BPF and its higher harmonics.

At first glance there is no explanation for the existence of those flow structures. The inlet nozzle and the radial gap between nozzle and the impeller front shroud are kept symmetric to a high degree of accuracy, inlet guide vanes do not exist. Therefore, the impeller operates under spatially extreme uniform inflow conditions. Thus, a thorough understanding of the phenomenon requires unveiling the flow structures in more detail. This is done by a numerical analysis of the unsteady flow in the impeller and flow visualization with smoke.

5. NUMERICAL ANALYSIS AND FLOW VISUALIZATION

5.1 Code and set up

A 3D unsteady numerical simulation of the flow through the impeller is performed. The hybrid SAS method (Scale Adaptive Simulation) had been selected. The SAS is a modified DES (Detached Eddy Simulation) method which provides a LES (Large Eddy Simulation)-like behaviour in detached flows. The turbulence model used is the Shear-Stress-Transport (SST) model. Unsteady parts of the flow field are solved with a second-order central difference scheme, otherwise a second-order upwind scheme with numerical advection correction is used. The time integration is done by a second order backward Euler scheme. A detailed description of the SAS is given in [24, 25]. The scheme is implemented in the commercial flow solver ANSYS CFX® 11.0 which is used throughout this study. The computational domain is a simplified representation of the test rig, Fig. 16. The numerical grid consists of 1.64 million hexahedron elements. The computational domain is divided into three domains: The non-rotating inlet, the rotating impeller and the non-rotating outlet. All surfaces between rotating and non-rotating domains are connected via interfaces. At the inlet the mass flow rate is specified in terms of density and flow velocity normal to the surface such that the impeller operates at its design point, i.e. at $\varphi_{r,\mathrm{opt}}$ = 0.15. Also a medium degree of turbulence has been selected at the inlet. The cylindrical boundary of the large inlet-domain, the inlet nozzle, all wetted impeller surfaces and the boundaries of the pressure chamber including the walls of the simplified drive are modelled as no slip walls. The fluid leaves the system

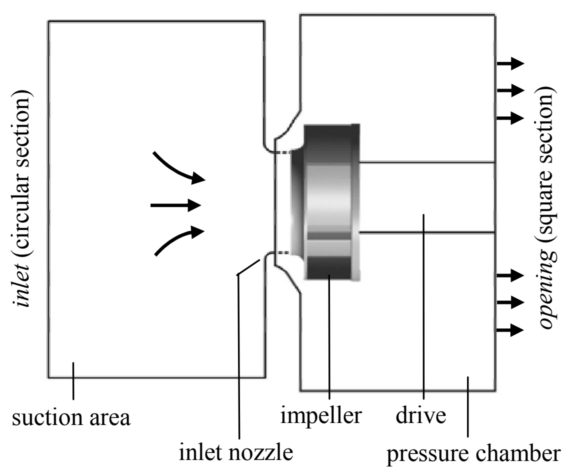

Fig. 16. Numerical simulation: computational domain

at the outlet of the pressure chamber, where an opening boundary condition with the static pressure set to 0 Pa has been specified. The time increment is set such that 2,273 time steps correspond to one revolution of the impeller. Because of the CPU time required the simulation was limited to 11,365 time steps, resulting in a total simulation time of 0.2273 s or five revolutions of the impeller.

5.2 Results

Fig. 17 shows an instantaneous picture of the streamlines far upstream of the impeller intake. Time instances referred to are summarized in Tab. 3. The flow velocity increases gradually along the streamlines. The isosurfaces of the velocity are nearly hemispheres. This proves that the inflow is symmetric and undisturbed. However, as the flow enters the impeller intake, gradually a pre-swirl is imposed on the inflow. In the centre region the streamlines begin to curl.

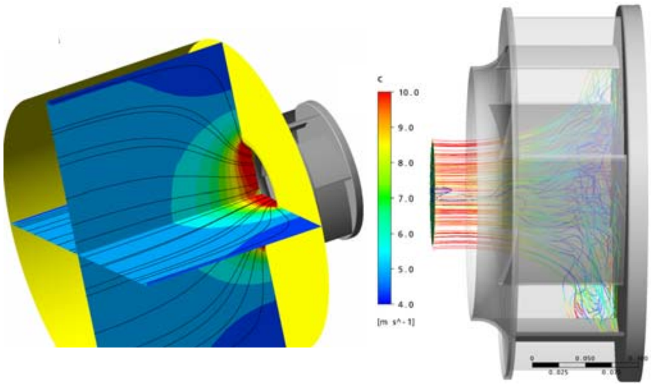

Fig. 17. Instantaneous streamlines at t_4; left: upstream of the impeller intake, right: in the centre region of impeller intake

Tab. 3. Time instances and angular impeller position for numerical data analysis

Time instance	Time increment [10^{-3} s]	Angular impeller position [°]
t_1	0	0
t_2	6.77	60
t_3	11.7	105
t_4	16.7	150
t_5	21.7	195
t_6	56.7	510

Of further interest is the frequency associated with the vortex and its spin. In Fig. 20 the predicted blade pressure fluctuation at a monitored point on the blade is compared with a measured time signal. The dominant frequency compares favourably, while the amplitude shows some differences. Nevertheless, the numerical prediction seemingly represents the key phenomenon in the intake flow field. Further validation of the numerical results was obtained by averaging the pressures at the intake and discharge with respect to space and time. The impeller overall pressure rise as predicted by the numerical simulation is very close the measurement, Fig. 4.

6. SUMMARY AND CONCLUSION

As in any centrifugal impeller the fluid at the intake is deflected from a purely axial into a radial direction. This does not happen abruptly as the fluid passes the blade leading edges. The blades and the friction of the rotating hub gradually impose a pre-swirl on the inflow and cause the formation of an inlet vortex. A key result of this study is that in the impellers investigated this inlet vortex is not stable. It takes a helical form, with the vortex core varying slowly its position with respect to the impeller center. Also the vortex strength varies with time. The characteristic frequencies associated with the vortex movement are very small as compared to the blade speed. In fact, the vortex structure can be considered as being nearly stationary for small time intervals. Thus, the blades cut through the quasi-stationary helical vortex each time it meets a trailing edge. This is the reason for strong blade surface pressure and hence force fluctuations which eventually act as sources for tones produced at BPF. On the other hand the slow spin of the vortex core and the slow variation of vortex strength are responsible for the amplitude modulation of the BPF tone as observed and clearly audible in the experiments.

Reducing the tonal noise at blade passing frequency and its higher harmonics would require a design which is substantially free from an unstable inlet vortex. Much current knowledge of the stability of swirling flows is based on studies in pipes. Stability criterions are the ratio of axial to circumferential flow velocity and their radial distributions. However, the formation of the vortex in the intake of a centrifugal impeller seemingly is more complex. Chen et al. [26] refer to an inlet vortex, however due to inlet guide vanes. More likely the vortex structure detected here is related to the draft tube vortex found in water turbines or in the intake of pumps (Gülich [27]). Further effort is required to link the geometric design parameters such as intake or width to impeller diameter ratio and aerodynamic non-dimensional coefficients to the existence of a stable or unstable inflow, which in consequence, is essential for a low noise fan design.

ACKNOWLEDGEMENTS

This investigation was partly funded by the German Federal Ministry of Economics and Technology (BMWi) via the consortium for industrial research "Otto von Guericke" (AiF) under grant 14611N/1 and the Forschungsvereinigung Luft- und Trocknungstechnik e.V. (FLT).

REFERENCES

[1] K.-R. Fehse, W. Neise, Generation mechanisms of low-frequency centrifugal fan noise. AIAA-Paper AIAA-98-2370, 1998

[2] J.-S. Choi, D. K. McLaughlin, D. E. Thompson, Experiments on the unsteady flow field and noise generation in a centrifugal pump impeller. Journal of Sound and Vibration 263, pp. 493-514, 2003

[3] M. Gottschalk, Untersuchung der Kennlinienstetigkeit von Radialventilatoren (Investigation of discontinuous performance curves of centrifugal fans). Strömungsmechanik und Strömungsmaschinen, Heft 17 September 1974, Verlag G. Braun Karlsruhe, 1974

[4] L. Mongeau, D.E. Thompson, D.K. McLaughlin, Sound generation by rotating stall in centrifugal turbomachines. Journal of Sound and Vibration 163(1), pp. 1-30, 1993

[5] L. Mongeau, D.E. Thompson, D.K. McLaughlin, A method for characterizing aerodynamic sound sources in turbomachines. Journal of Sound and Vibration 181 (3), 369-389, 1995

[6] L.G. Tetu, D.K. McLaughlin, D.E. Thompson, Noise produced by large scale instability modes in centrifugal turbomachinery, Proceedings of the ASME Noise Control and Acoustics Division, NCA-Vol. 21, 1995

[7] P. Fringe, R. Van den Braembussche, A theoretical model for rotating stall in the vaneless diffuser of a centrifugal compressor. Journal of Engineering for Gas Turbines and Power, Vol. 107, pp. 507-513, 1985

[8] G. Pavesi, G. Cavazzani, G. Ardizzon, Time-frequency characterization of the unsteady phenomena in a centrifugal pump. International Journal of Heat and Fluid Flow 29, pp. 1527-1540, 2008

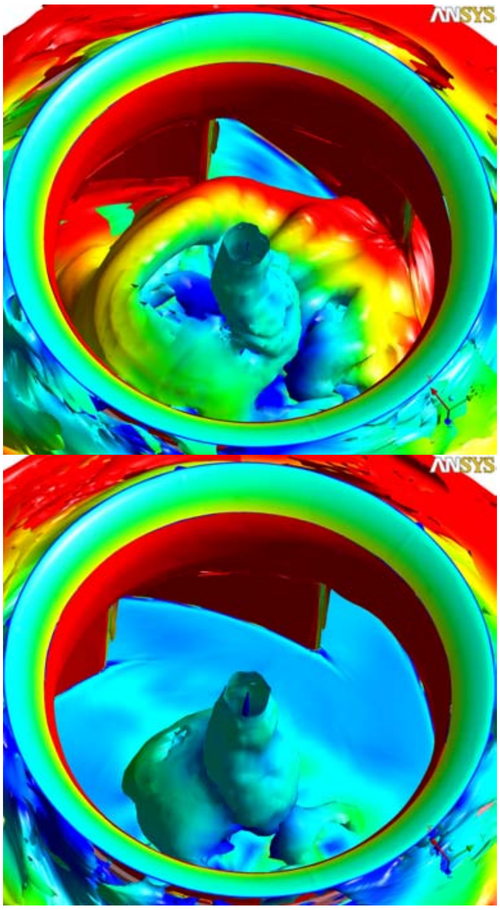

Fig. 18. Isovorticity surface at impeller intake (500 s^{-1}, scaled with the relative flow velocity) at time instance t_1 (upper) and t_6 (lower)

[9] T. Carolus, D.K. McLaughlin, R. Basile, Experimental investigation of the unsteady discharge flow field and the noise of a centrifugal fan impeller. Proceedings of the 7th International Congress on Sound and Vibration, Garmisch-Partenkirchen, Germany, 2000

[10] D. Wolfram, Th. Carolus, Akustische Quellen bei gehäuselosen Radialventilatoren: Analyse, Modelle, Minderung (Acoustic sources in isolated centrifugal fans: Analysis, models, reduction). Report No. F20910A by the Institut für Fluid- und Thermodynamik, Universität Siegen, 2009

[11] Radialventilator und Düse für einen Radialventilator (Centrifugal fan and inlet nozzle). Deutsche Gebrauchsmusterschrift DE 200 01 746 U 1, June 21, 2001

[12] M.V. Lowson, The sound field for singularities in motion. Proceedings of the Royal Society, London, A 286 (559-572), 1965

[13] S.E. Wright, The acoustic spectrum of axial flow machines. Journal of Sound and Vibration 45, pp. 165-223, 1976

[14] M. Roger, Noise in Turbomachines – Noise from moving surfaces. VKI-Lecture Series 2000-02, von Karman Institute for Fluid Dynamics, Belgium, 2000

[15] M.E. Goldstein, Aeroacoustics. McGraw-Hill, 1974

[16] W.K. Blake, Mechanics of flow induced sound and vibration. Academic Press Inc., 1986

[17] DIN 24163, Ventilatoren, Teil 2: Leistungsmessung - Normprüfstände (Fans, part 2: performance tests - standardized test rigs). Deutsche Norm, 1985

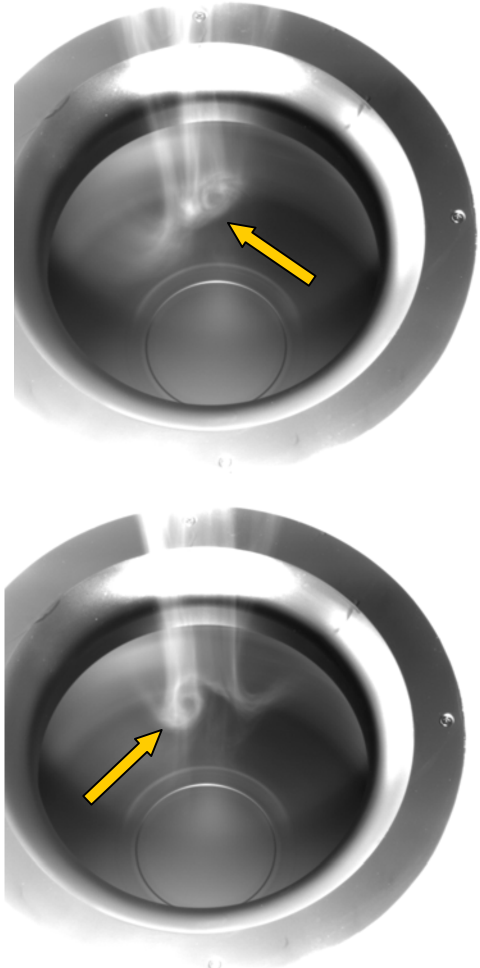

Fig. 19. Snapshots of a smoke filament at impeller intake at two different time instances

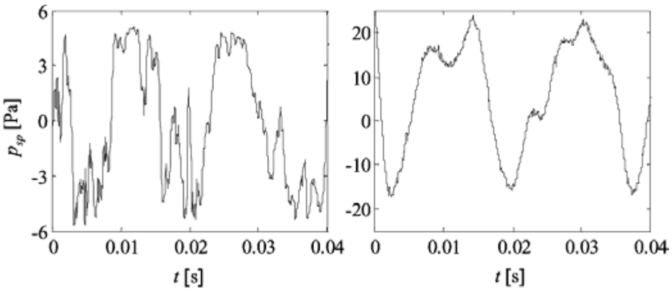

Fig. 20. Time record of blade surface pressure fluctuation at monitoring point ξ_{11} = 0.9, ξ_3 = 0.03; left: measurement; right: numerical prediction

[18] J. Weidemann, Beitrag zur Analyse der Beziehungen zwischen den akustischen und strömungstechnischen Parametern am Beispiel geometrisch ähnlicher Radialventilator-Laufräder (A contribution to the analysis of the relationship between acoustic and aerodynamic parameters for geometrically similar centrifugal fan impellers). DLR-Forschungsbericht 71-12, 1971

[19] P.H. Bent, Experiments on the aerodynamic generation of noise in centrifugal turbomachinery. PhD Thesis, Pennsylvania State University, 1993
[20] L.G. Tetu, D.K. McLaughlin, D.E. Thompson, Noise produced by large scale instability modes in centrifugal turbomachinery, Proceedings of the ASME Noise Control and Acoustics Division, NCA-Vol. 21, 1995
[21] J.S. Bendat, A.G. Piersol, Engineering applications of correlation and spectral analysis. John Wiley & Sons, Inc., 1993
[22] D. Wolfram, Analyse des Entstehungsmechanismus von Drehtönen bei gehäuselosen Radialventilatoren (Analysis of the blade passing frequency tone mechanism in isolated centrifugal fan impellers). Fortschritt-Bericht VDI Reihe 7 Nr. 496, VDI-Verlag, 2009
[23] Wolfram, D., Carolus, T.: Experimental and numerical investigation of the unsteady flow field and tone generation in an isolated centrifugal fan impeller. Journal of Sound and Vibration 329 (2010) 4380-4397
[24] F.R. Menter, M. Kuntz, R. Bender, A scale adaptive simulation model for turbulent flow predictions. AIAA Paper, AIAA2003-0767, 2003
[25] F.R. Menter, Y. Egorov, A scale-adaptive simulation model using two-equation models. AIAA Paper, AIAA2005-1095, 2005
[26] P. Chen, M. Soundra-Nayagan, H.C. Simpson, Unstable flows in centrifugal fans. Proceedings of the IMechE 1992-3, pp. 25-32., 1992
[27] J.F. Gülich, Kreiselpumpen. Springer-Verlag, 2. Edition, 2004

